LA-UR-05-1533

Approved for public release; distribution is unlimited.

Title: Fission Cross Sections of 240-Pu, 243-Am, 209-Bi, nat-W Induced by Neutrons up to 500 MeV Measured Relative to 235-U

Author(s): A. V. Fomichev, V. N. Dushin, S. M. Soloviev, A. A. Fomichev, S. G. Mashnik

Submitted to: General Distribution

A. V. Fomichev[1], V. N. Dushin[1], S. M. Soloviev[1],
A. A. Fomichev[2], S. G. Mashnik[3]

Fission Cross Sections of ^{240}Pu, ^{243}Am, ^{209}Bi, ^{nat}W Induced by Neutrons up to 500 MeV Measured Relative to ^{235}U

[1]V. G. Khlopin Radium Institute, 2nd Murinsky 28, Saint-Petersburg, 194021, Russia

[2]Saint-Petersburg State University, St.-Petersburg, 198504, Russia

[3]X-5, Los Alamos National Laboratory, Los Alamos, NM 87545, USA

Abstract

Results of recent measurements carried out at the spallation neutron source of PNPI, Gatchina, Russia, are presented. Contrary to our previous works, the data processing procedure is described in details. Fission cross section values derived from experimental data are presented in four tables. The measured cross sections for americium, plutonium, bismuth, and tungsten are analyzed with an improved version of the Cascade Exciton Model as realized in the code CEM03.

I. INTRODUCTION

The use of pulsed spallation neutron sources in measuring nuclear reaction characteristics allows us to obtain data in a wide range of neutron energies. In this way, one obtains the measured values as a function of the energy of neutrons inducing the reaction. This is an additional advantage that might be used to test various nuclear models and to check computer codes used in various applications.

The disadvantage of this method is a necessity to use large flight paths, which lowers considerably the density of neutron flux incident on the target. This is a serious obstacle for multi-parameter experiments and measurements for target nuclei with low fissility.

However, experiments with low-fissility nuclei are of special interest. When the fission cross-section decreases by several orders of magnitude down to the level of other reaction channels competing with the fission one, there appears an additional possibility to gain nuclear information, since the shape of the fission cross-section curve as a function of neutron energy would be sensitive to opening of those channels.

II. EXPERIMENTAL PROCEDURE

The measurements were performed on a 50-meter flight path of GNEIS facility of PNPI [1]. An 1 GeV pulsed proton beam strikes a lead target, producing neutrons by spallation reactions.

A multi plate ionization chamber was the fission detector. The preamplifiers were located on the outer plugs. The anode signals, which were pulses of 170 ns width and have 20 ns leading edge, were dispatched to the distance 1.5 m for data acquisition station. The detector assembly in the neutron beam is shown in Fig. 1.

The data acquisition system was an assembly of CAMAC units. A signal, coming from detector lines, was digitized with a step of 10 ns. A PC computer read digital output. Further, this computer and the CAMAC controller performed the data processing as well. The accumulated time-of-flight spectra, shape of detector's pulses, electronic noise, the shape of gamma flash and other necessary parameters one could be seen on the display.

The data acquisition system made the pulse height analysis of detector signals. The time-of-flight technique was used to measure the incident neutron energy.

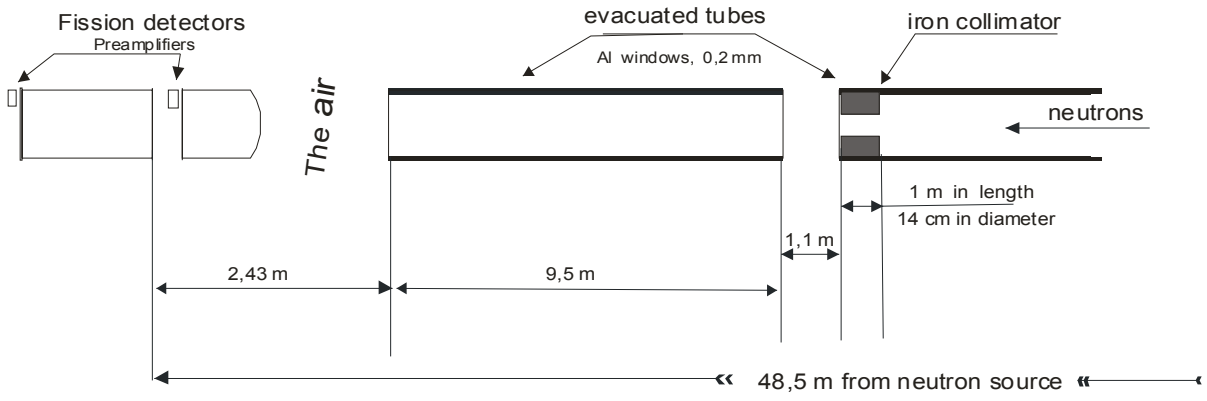

Fig. 1. Layout of the experimental setup.

III. DATA PROCESSING

1. Time-energy scale calibration

One of the key problems of data processing is transformation of the time scale of data files into the energy scale. The reliability of final fission cross section values depends on the accuracy of this procedure.

A start signal, synchronized with the accelerator, starts up the data acquisition system. The system begins to process the detector signals and stops after 5.12 μs. The data acquisition system digitizes the input signal with a step of 10 ns. The time channel widths are strongly equal each other, since they are set by a quartz generator and their total number is 512. This number is restricted by the size of electronic memory cells. The computer program finds fission pulses (with amplitude above the threshold) and puts them into a corresponding time channel. Thus, the accumulated data are a file consisting of 512 numbers, which reflects the time distribution of detector signals, i.e. the time spectrum. An example of such a data file is shown in Fig. 1.

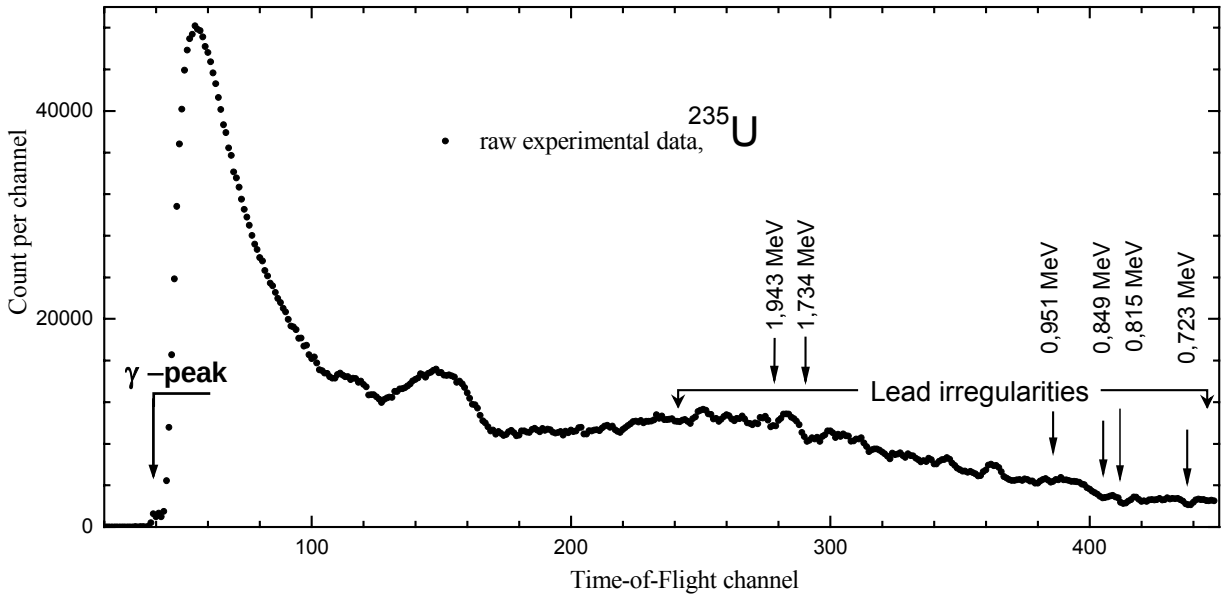

Fig. 2. Count rate of fission detector, i.e. time-of-flight spectrum.

The relation between the number of time channel and the energy of a neutron that induce this fission signal is given by the following relativistic equation

$$E_k = E_0[1/(1-\beta_k^2)^{1/2} - 1], \quad (1)$$

where,

$\boldsymbol{\beta_k} = L/t_k$, $t_k = k * 10\text{нс} + t_0$,

$\mathbf{E_k}$ is neutron energy,

k is the channel number (varied from 1 to 512; in reality, from 40 up to 480),

$\mathbf{t_0}$ is start time shift,

L is the distance between the detector and the neutron source,

$\mathbf{E_0}$ is a constant.

Two parameters of this equation, L (flight path) and t_0 (time shift), are not measured in the experiment directly. However, it is possible to evaluate these parameters using the distinctive features of the shape of time-of-flight spectra.

The first feature is a peak caused by fission induced by γ-quanta (arising from the neutron-producing target). This peak is located in the beginning of the spectrum, i.e. corresponds to the first time channels (about 170 nsec from the "zero" time in our case). The position of the center of this peak (Fig. 1) indicates the channel number where the γ-quantum came to the fission detector camera. Widths of this peak show the behavior of the fission detector time-resolution functions.

Another type of features are separate uprises and downwards in the shape of spectra that are well pronounced in their low-energy tails, i.e., in the channels with high numbers (about 300-400). These irregularities are caused by neutron

transport through lead target. They can be compared to the well-known shape of the energy dependence of the neutron total cross-section on lead (which is of resonance feature in this range), so that we can obtain the values of neutron energies for some part of the time channels with high numbers. This step of energy scale calibration is illustrated in Fig. 3.

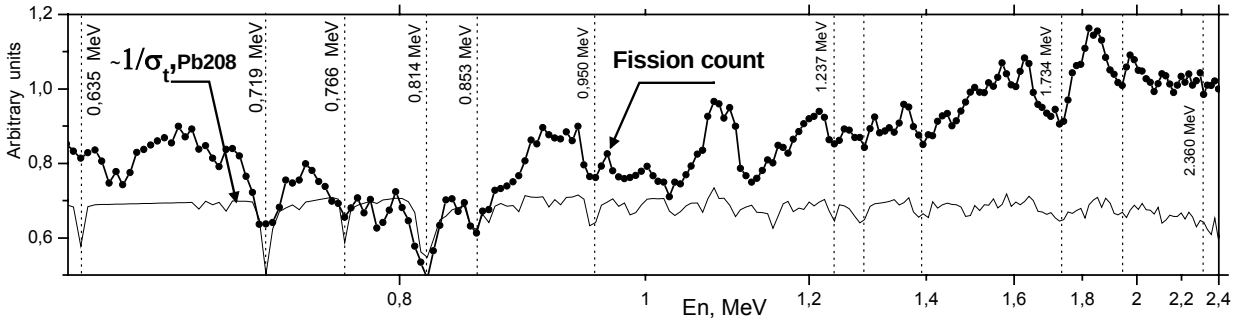

Fig. 3. Referencing the energy scale by comparison the shape of the experimental spectrum with the shape of the energy dependence of the lead total neutron cross -section [2].

We have computed the covariance function between the experimental spectrum and the total neutron cross-section curve, and, on the basis of this function, ascribe to the time channel any energy value from the total neutron cross section curve. It may be assumed the accuracy of such ascription procedure is of 5 ns (half of the time channel width). Usually, we use 4-6 ascribed energies vs. channel-number points.

To get the gamma-position with a high accuracy, we implement a numerical procedure of subtracting the instrumental resolution function from the measured time-of-flight spectra. According to the operation parameters of the accelerator, the pulse length of a proton incident on the neutron-producing target is 10 ns. The variance of the interaction time of 1-GeV proton with the target with limited

size (20 cm) is less than 1-2 ns. Therefore, the actual length of γ-flash is about 10 ns. However, in our experiments, the instrumental function width is greater, approximately up to 19 ns.

To subtract the instrumental resolution function we solve the well-known convolution integral equation of the first kind

$$\int_{-\infty}^{\infty} A(t-\tau) \bullet \Psi(\tau) d\tau = \Phi(t), \qquad (2)$$

where

Φ(t) is the experimental time-dependent spectrum measured with a finite resolution,

Ψ(t) is the initial spectrum,

A(t) is the instrumental function, in most cases, a Gaussian:

$$A(t-\tau) \propto \exp(-(t-\tau)^2 / 2\sigma^2).$$

To obtain a stable solution of equation (2), Ψ(t), we used the Tikhonov method of statistical regularization [3]. The initial spectrum was specified with a 10-ns step, the output spectrum, with 5-ns step. The width (dispersion parameter - σ) of the instrumental function was specified approximately equal to a half of the experimental resolution and the smoothness and boundedness parameters were chosen so that the dip between the γ-peak and the remaining neutron part of the spectrum, well pronounced in a little part of series of measurements, be adequately described.

The time resolution unfolding is illustrated in Fig. 4. Black solid circles are experimental data. Open circles correspond to the result of reconstruction. Four examples of exposure Runs # 1, 2, 3, and 4, and four examples of unfolding spectrum are shown.

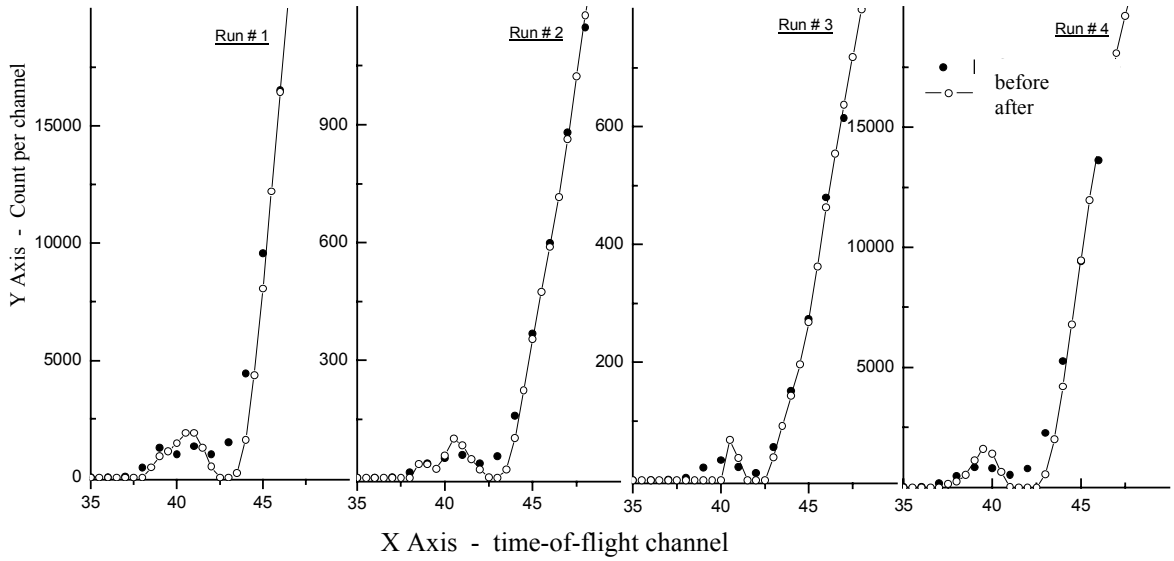

Fig. 4. Time resolution unfolding.

The mathematical procedure of energy calibration involved generation of a system of linear equations based on expression (2) and a solution of this system by the least square technique with respect to unknown parameters (2 parameters and 4-7 equations). This procedure allows to determine the flight path L with an accuracy of about 4 cm. Considering the fact that the size of the neutron-producing target are several times greater than this value, this accuracy is found to be sufficient. It should be noted that certain time-of-flight spectra could be interpreted as a demonstration of dependence of L on neutron energy. The shift of the start time point t_0 can be determined with an accuracy of 2 ns, which is sufficient at a width of the time channels 10 ns.

Thus, transformation of the time scale to the energy scale gives us the energy spectrum of accumulated signals, i.e. 512 values of neutron energy. The result of transformation time→energy is shown in Fig. 5. Each step in the figure corresponds to a certain time channel. The height of the step indicates the

number of counts in this channel and the step width corresponds to the width of a time channel expressed in MeV. At a constant width of a time channel equal to 10 ns, the width of corresponding range of neutron energy is variable. At the beginning of our energy range, it is up to 40 MeV, and at the end, of about 3 keV.

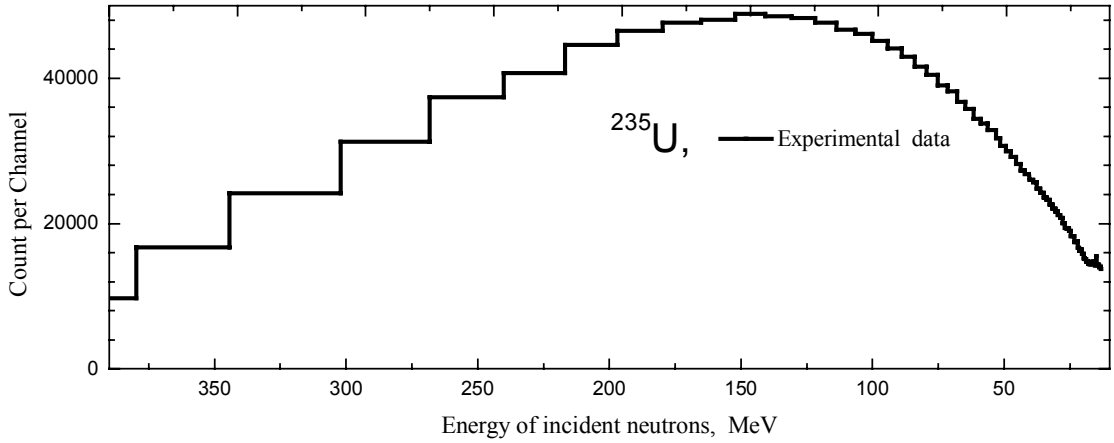

Fig. 5. The counts per channel of the fission detector after transformation of flight time to neutron energy.

2. Amplitude spectra treatment

In the course of detector signal registration, the CAMAC controller records both the time of its delivery and its amplitude. Thus, the experimental data present a two-parameter data file. These data allow us to construct: (a) the total amplitude spectrum of the signals corresponding to the given isotope layer, (b) the total time-flight spectrum, and (c) 128 amplitude spectra corresponding to 512 time channels.

The total spectrum was displayed during the experiment and was used for monitoring the operation parameters of the equipment. The spectra of the isotope layer tracks were constructed and analyzed during data processing after

completion of measurements. They are a kind of documentation for each point of the time spectrum presented in Fig. 2.

The aim of amplitude analysis is a separation of the desired fission signals from the noise and background signals. In so doing, simple and difficult cases can take place depending on the signal/noise ratio measuring tracks.

In a simple case, the peak(s) corresponding to fission events is well pronounced and is separated by a deep dip from the background signals. In this case, the problem is solved by extrapolation of the background section of the spectrum to the range of fission peak(s) and by extrapolation of the left slope of a fission peak to the range of noise signals. Linear and exponential extrapolations can be used. Typical values of corrections for the loss of the count of fission events (fission events below the discriminating threshold and background events above the threshold) are approximately of 1.2 - 2 % for U, Pu, Am targets. In our experiments, we have this case for nuclei with high cross-section (approximately 1 barn) and low intrinsic α-activity (half-life more than 10^5 years). In our case, this situation is realized for ^{232}Th, ^{238}U, ^{235}U, and ^{237}Np nuclei and is illustrated in Fig. 6.

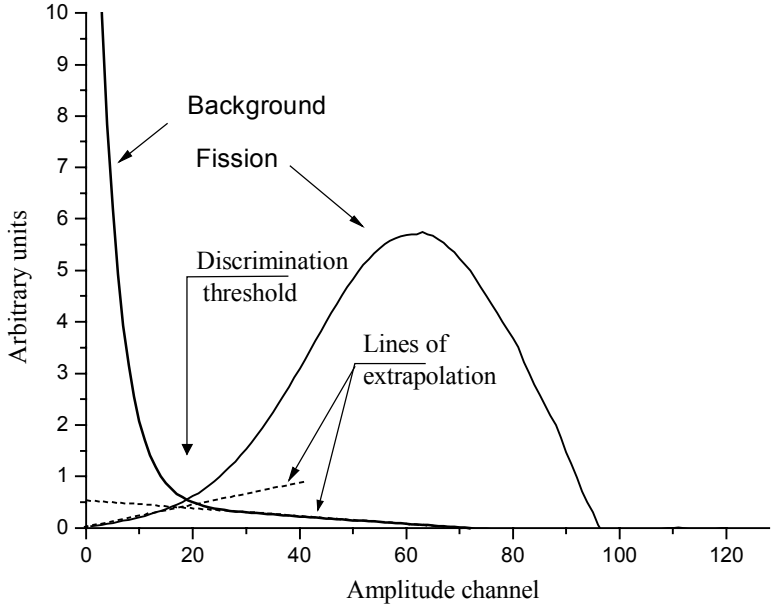

Fig. 6. Search of correction for the fission count by extrapolation.

When considering isotopes with high α-activity, such as ^{240}Pu and ^{243}Am, and poorly fissionable nuclei, such as tungsten, bismuth or lead, the problem of selection of the desired signal becomes more complicated. The values of extrapolation corrections increase dramatically, reaching for lead and bismuth up to more than 10 – 15 % and up to 60% for tungsten. This situation is illustrated by Fig. 7, which presents amplitude spectra of signals obtained in one of our experimental series from four different targets, U, Pu, Pb, and W, respectively.

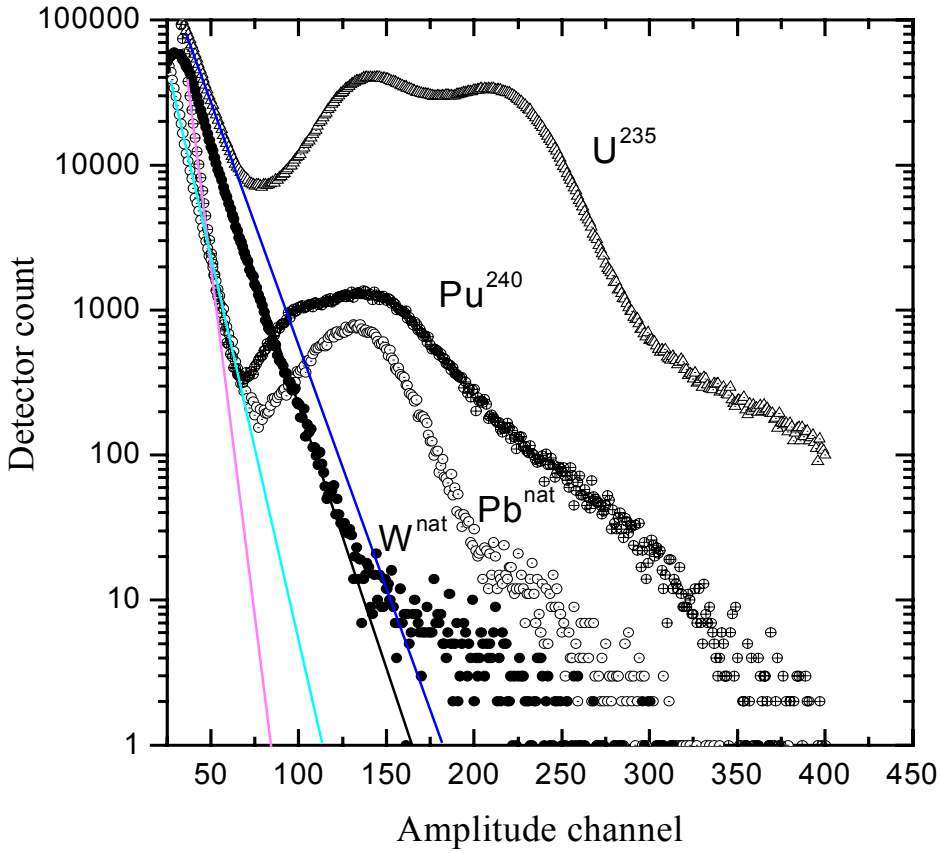

Fig. 7. Experimental amplitude spectra. Lines are extrapolation of the background parts of spectra.

It is seen that in passing from the uranium target to the tungsten target the fission peak becomes poorly separated from background events and the count of fission events decreases by thousands of times. We have calculated the energy-

release in gas due to reactions as Al(n,xp+yd+zt+wα)X. Our estimations show that the background spectrum can be explained (at least, above the channel # 35, i.e., about 7 MeV) as an energy-release of charged particles from neutron reactions on structural supporting material. Computations reproduce the slope of the background part of spectrum with high quality and the absolute value of the background with a factor two of accuracy. So, we treat the different slope of the straight lines of background approximation as caused by different multiplication factors of measuring tracks.

It is seen from Fig. 7 that the spectra of tungsten targets do not exhibit a fission peak: its left slope is confluent with the background. Therefore, we have a possibility of extrapolation of only background events. This extrapolation allows us to assign the events located to the right side of the straight line in Fig. 7 to fission events. However, the number of fission events located to the left side of this straight line cannot be determined. In other words, the spectrum shape does not contain information on efficiency of registration of fission events with the detector.

We have a very limited information on the shape of fission fragment spectrum of tungsten, i.e.: (a) the amplitude spectrum of fission signals has a one-hump bell-shaped curve, (b) its shape should be similar to the spectra of Pb and Bi, and (c) the average amplitude of fission signals of tungsten is less than that of these nuclides.

We have decided to process tungsten spectra on the basis of a calculation model of the instrumental amplitude spectra. To attain this purpose, we worked out a model being applied to relations, recommendations, and parameters from the GEANT4 [4] and GEM [5] codes, and a RIPL project. The experimental amplitude spectra of bismuth and lead obtained on our installation can be used for verification and comparison of model results.

The following processes were considered:

1) Excitation of a nucleus due to the energy of the incident neutrons;
2) Nucleon evaporation before fission;
3) Formation of mass and charge distributions of fission fragments;
4) Energy release in fission on the basis of nuclear masses;
5) Distribution of kinetic energy among fission fragments;
6) Ionization energy loss of fragments in fissile layers of the target;
7) Ionization energy loss of fragments in gas.

We used recommended values for the mass and charge distributions of fission fragments from [6], the total energy release in fission from [7], the level density (slightly corrected by experimental data on neutron multiplicity of Cf252 Sf fragments) from [8], and the range of fission fragments from [9].

The elaborated model contains one natural parameter (vector), which allows us to reproduce the shape of experimental amplitude distributions for Bi and Pb. This parameter is the spectrum of nuclear excitation energy before fission. The results of simulation are shown in Figs. 8a and 8b, which present evaluated curves and experimental data. The experimental data in Fig. 8a are presented after subtraction of the exponential background (80 and lower amplitude channels).

The model parameters were verified on reproducing the experimental data for lead and bismuth, and used for evaluation of the amplitude distribution for tungsten. In so doing, only one of these parameters, the excitation energy spectrum of fissile nucleus, was varied. We note that the excitation energy spectrum was relatively stronger for W than for Bi or Pb. As a result of these calculations, we obtained the shape of the desired signals from the tungsten target, required for background subtraction.

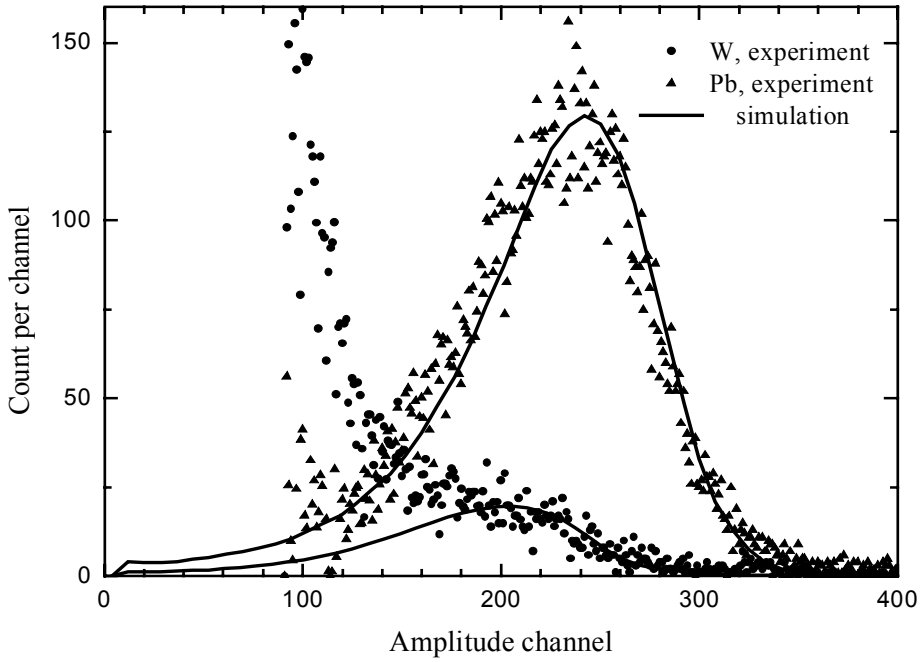

Fig. 8a. Amplitude spectra of tungsten and lead targets and the results of simulation. Lead data present two different series with different gas pressure.

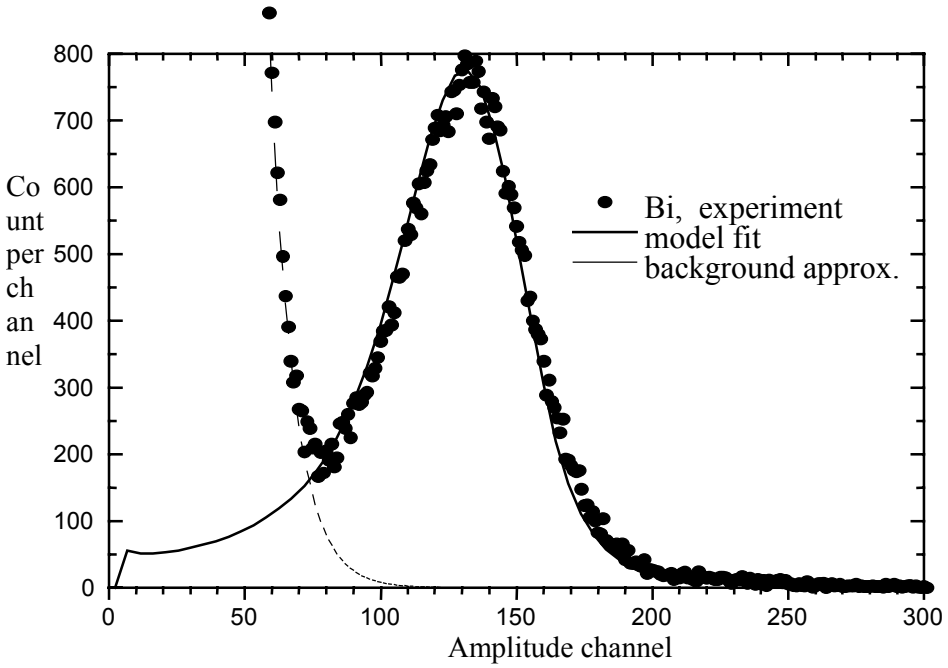

Fig. 8b. Amplitude spectra of signals from bismuth target and results of our simulation.

The result of using this approach is shown in Fig. 9. The amplitude channel, in which the discrimination threshold is established, is plotted on the abscissa. The numbers of fission events are plotted as ordinates. Line 1 shows the sum of the found fission events in the case when only exponential extrapolation above the discrimination threshold is used. Line 2 shows the corrected sum of found fission events with the use of evaluated shape of the spectrum of fission signals for extrapolation to the range below the discrimination threshold. Line 1 has a big slope while line 2 is located in a fairly narrow range. The range width (type of discrimination plateau) is about 5%. This value can be taken as the error in determination of the efficiency of fission detector in measurement with tungsten.

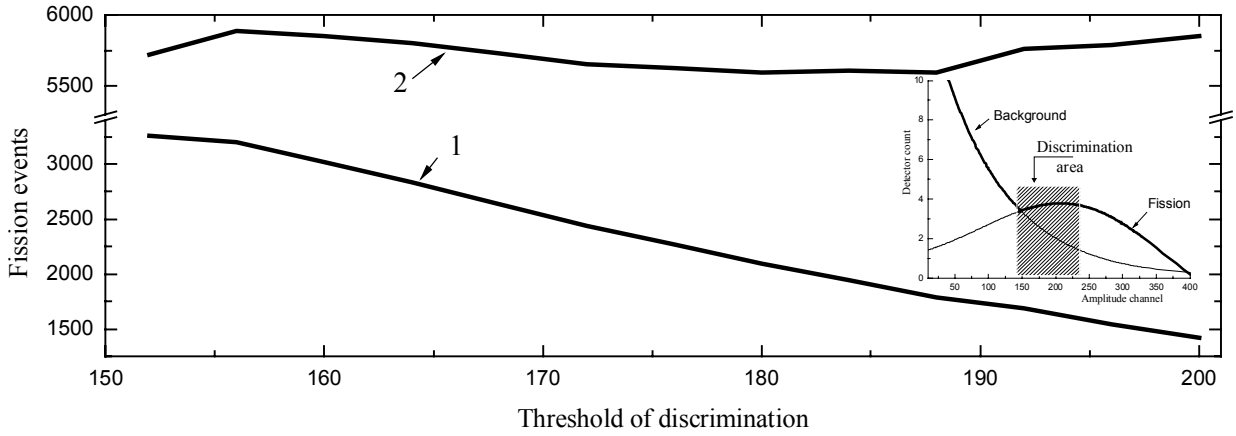

Fig. 9. Plateau of discrimination for tungsten: (1) Amount of fission events, exponent extrapolation of background only; (2) Corrected amount of fission events with the use of evaluated shape of the amplitude spectrum of fission signals.

3. Neutron flux attenuation

The neutron beam, in which the fission detectors are placed, interacts with the detector structural and supporting materials. Two types of processes can occur: (a) loss of neutrons with primary energy, and (b) generation of secondary neutrons (and other particles).

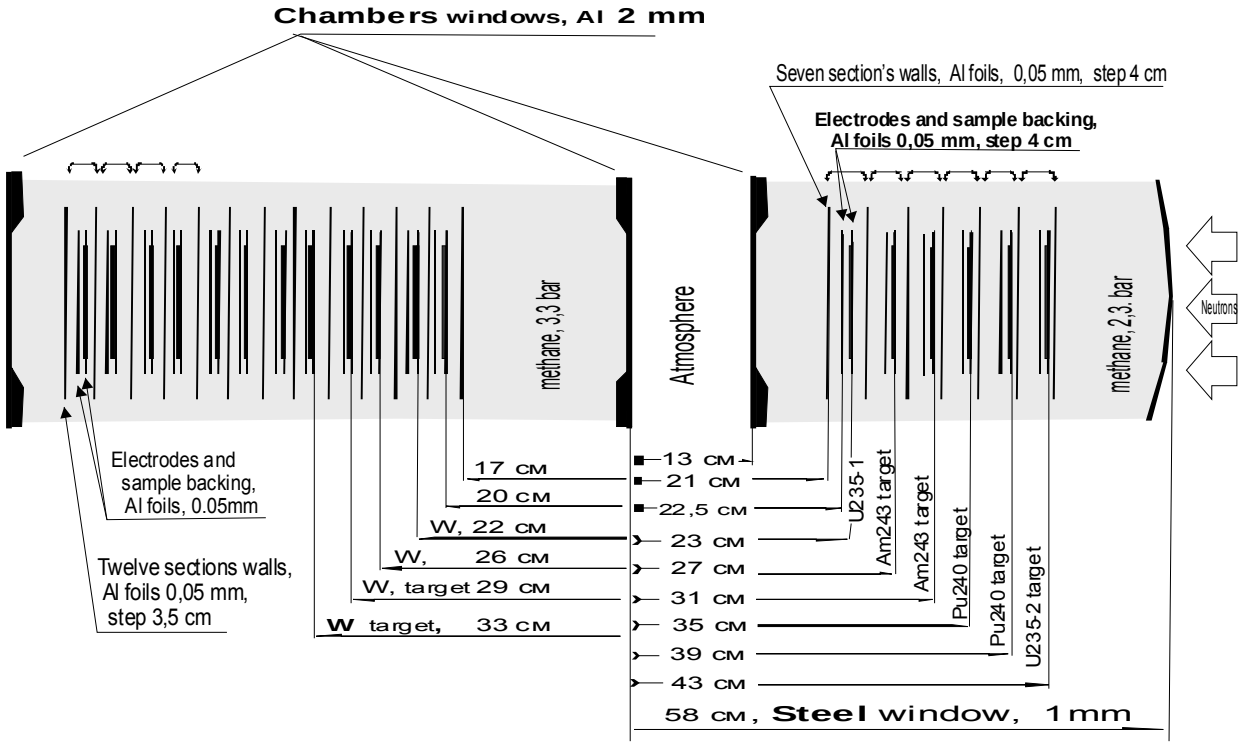

Fig. 10. Arrangement of fissile layers and construction elements of ionization chambers in the neutron flux, used for calculation of corrections. The right part is the "W-camera" and the left part, the "Actinide-camera"

We performed calculations that allow us to estimate the parameters of these two processes and to make the necessary corrections. Fig. 11 shows how the number of initial neutrons varies in passing from the first target which they meet on their path to the last target, i.e., the decrease of the initial neutron flux.

In Fig. 11, lines 1 and 2 show the loss of neutron flux in the first chamber, i.e., a decrease in the number of neutrons incident on the last target in the actinide chamber in comparison with the number of neutrons incident on the first target.

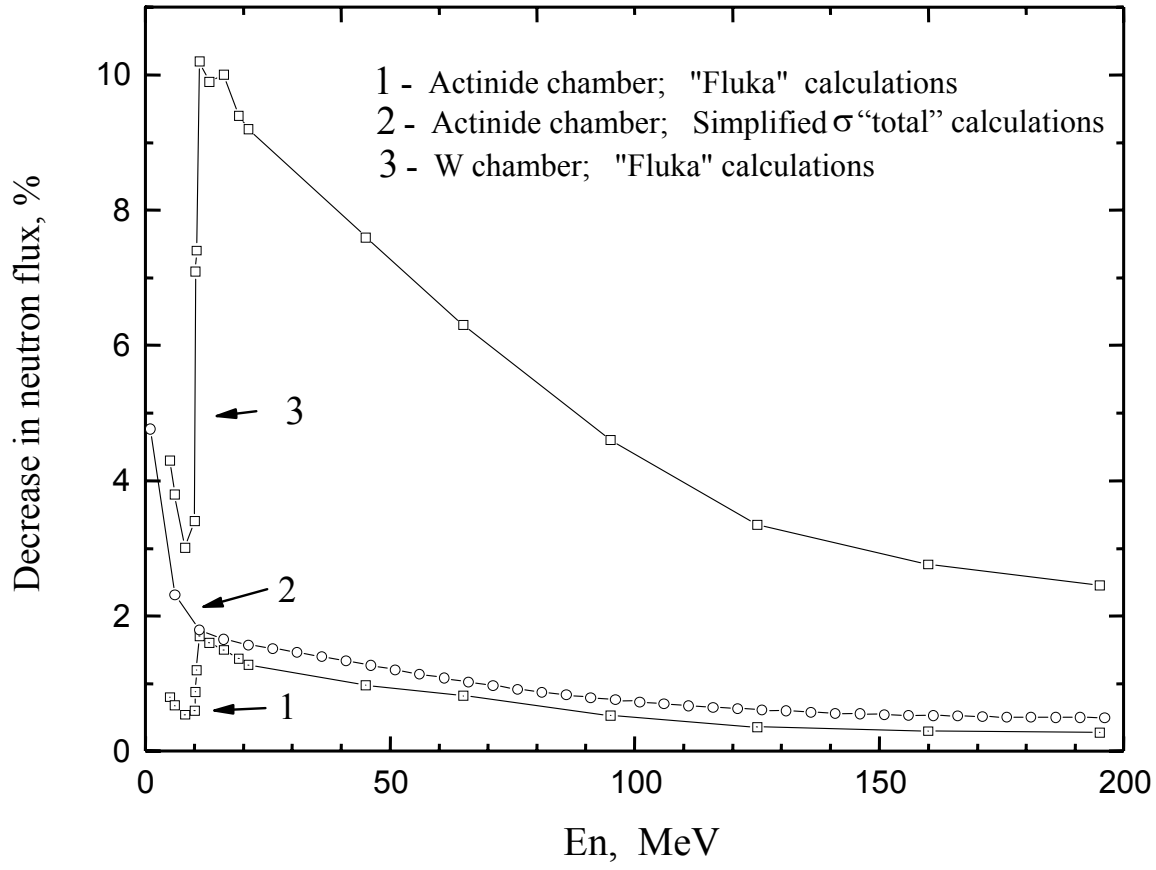

Fig. 11. Loss of neutron flux in construction materials of fission detectors.

Line 3 shows a further decrease in neutron flux along the path to the last target in the tungsten chamber. In calculations, two methods were used: (a) FLUKA code calculations [10] with a full geometry of fission detectors, shown by lines 1 and 3, and (b) taking into account only neutron flux attenuation due to the total cross-section of neutron interaction with construction materials, shown by line 2. Line 3 in Fig. 11 shows fairly noticeable loss of neutron flux as a result of interactions with the chamber's walls. A question arises: How the initial spectrum does change? These changes are represented in Fig. 12.

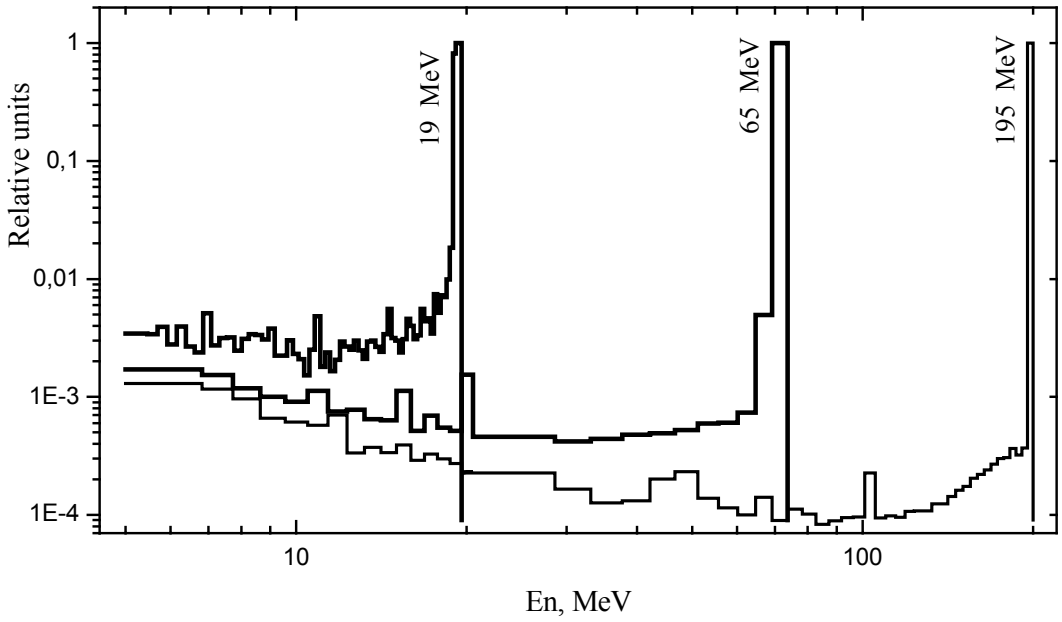

Fig. 12. Neutron spectra after passing through construction materials of the fission detectors according to FLUKA calculations for three monoenergetic groups of 19-, 65-, and 196-MeV neutrons, respectively.

This plot shows simulated spectra for three monoenergetic groups of 19-, 65-, and 195-MeV, when the flux passes through both ionization chambers, i.e., in the case of maximum decrease of the flux. Our estimations show that the correction for the number of fission events induced by neutrons with changed energy is in the range 0.3-0.6% for various flight-of-time channels.

IV. FISSION TARGETS

1. Introduction

The targets present aluminum foils with a thin layer of sprayed fissionable substance. The foils are fixed in the ring mount and serve as a cathode in the ionization chamber. The surface area of the fissionable layer is 250 cm^2, the thickness of the foil and the mount is 0.05 and 1 mm, respectively. The fissionable nuclei are contained in the layer of fissionable substance. The layer thickness is insufficient to produce a noticeable loss in the kinetic energy and

the amount of fragments. The typical content of fissionable nuclei in the target does not exceed 200 μg/cm^2 and the loss of the number of fragments in a layer is 1-3% for heavy nuclei.

2. Preparation

Actinide targets were prepared by applying a solution containing the nuclei to the surface of an aluminum foil by a brush. After drying the foil was calcined at approximately 200°C. As a result, at the foil surface a strong film of uranium, plutonium, or americium oxides is formed.

In preparation of an americium target, the initial sample was purified to remove Cm-244 impurities with the use of well-known chemical procedures. Purification was performed in two stages: precipitation of curium from a solution with ammonium hydroxide and passing of hot nitric acid solution of americium through a column filled with Dowex-50. At each stage, the degree of purification was monitored by α-spectrometry.

Tungsten targets were prepared in a similar way, i.e., by applying of ammonium tungsten solution to the surface of an aluminum foil with subsequent calcinations at 200°C.

Bismuth and lead targets were prepared by thermal atomization in vacuum on a UVR-50 setup.

3. Amount and uniformity of applied nuclide control

In preparation of radionuclide targets, the total amount of applied nuclei was determined by measuring the total α-activity of the target. The measurements were carried out in a vacuum chamber of 25 cm in diameter and 62 cm in height. A silicon detector with a calculated solid angle $\Omega=8.19\cdot10^{-5}$ sr was placed on the top cover of the chamber. The energy resolution of the α-spectrometric channel

allowed us to separate α-peaks related to various isotopes and to determine the content of impurity radionuclides in the targets. As an example, this spectrum is shown in Fig. 13.

The uniformity of the applied layer was monitored by measurement of distribution of radionuclide density at the target surface. A silicon detector was moved along the target surface at a distance of 2.8 cm from this surface. The uniformity was estimated from the count of α-particles from 13 sections of 15 mm in diameter each (spatial angle of $3.41 \cdot 10^{-3}$ sr). The average density of radionuclide determined by this procedure is in a good agreement with the results of measurement of the total α-activity of the target.

In preparation of bismuth and lead targets, the amount of applied nuclides was determined by a simple weighing of aluminum foil before and after thermal atomization. The uniform thickness of the layers was reached when the distance between the foil and the evaporator was fairly big.

To determine the thickness and uniformity of tungsten layers, we used a procedure developed at the Khlopin Radium Institute [11] based on the use of the Rutherford effect, backscattering of light charged particles. The target surface was irradiated with α-particles outgoing from a ring Po-210 source; a silicon detector of 10 mm in diameter was placed inside the ring. The measurements were performed as in the case of operation with active targets. The source and the mask (not 15, but 24 mm in diameter) were moved at the target surface. However, in this case, the silicon detector recorded not natural α activity of the target but the flux of Po-210 α-particles scattered by the target. The tungsten amount at the target was determined by the relative method, comparison with scattering from the reference target. The reference target was a U-238 target, for which the amount of uranium nuclei was determined from the natural α-activity.

The instrumental α-spectrum obtained in calibration of tungsten targets is shown in Fig.13. The peak in the beginning (left part) of each spectrum corresponds to α-particles scattered on aluminum foil. The peak in the right part of the spectrum corresponds to the background of the polonium source. The medium peak corresponds to α-particles scattered on tungsten and uranium nuclei, respectively. The count summed from 150 to 225 channels in the spectra (a) and (b) gives the density of tungsten or uranium layers.

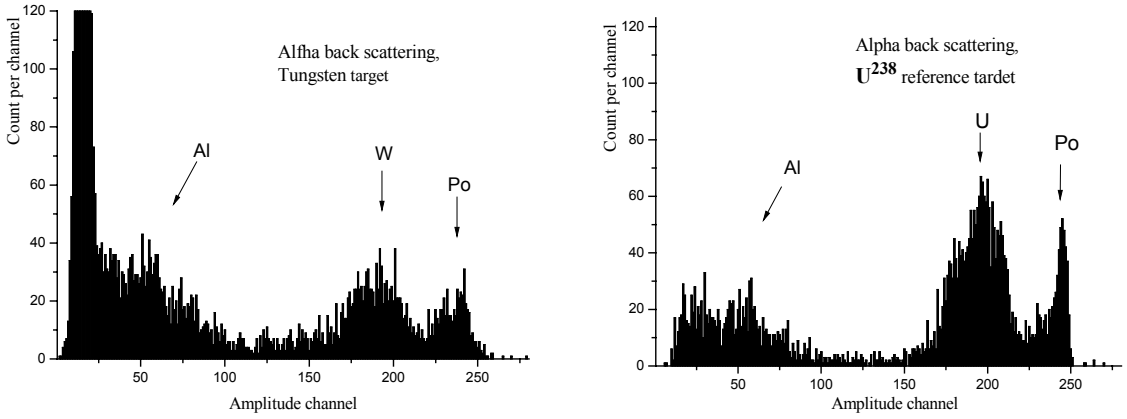

а) б)

Fig. 13. Spectra of ^{210}Po α-particles scattered in reverse direction from a tungsten target (a) and a reference target with the density of uranium layer of 0.53 mg/cm^2 (b).

The characteristics of the targets used in our experiments are listed in Table 1. Their order corresponds to the order of arrangement of targets along the neutron flux.

Table 1. Fission targets

Target	Layer thickness, **mg/cm^2**	Heterogeneity, **%**	Amount of radionuclide, **mg**	Fissionable admixtures, **%**
U235 - 2	0,157	0.8		≤0,008
Pu240 - 3	0,0044	12	1,11±0,06	≤0,12
Pu240	0,0052	9,4	1,32	2,73±0,53
Am243 - 1	0,0077	17	1,95±0,1	≤1,5
Am243 - 3	0,0055	17	1,40±0,07	≤1,5
U235 - 1	0,15	2,3	37,4±2.0	≤0,008
U235	0,26	4,7	67,1±2,0	≤0,008
Wnat - 111	0,107	16	27	
Wnatt - 117	0,127	12	32	
Wnat - 115	0,140	8	36	
Wnat - 114	0,150	25	39	
Wnat - 123	0,150	10	38	
Wnat - 116	0,156	4	40	
Wnat - 110	0,176	12	52	
Bi209 - 29	0,30		76,3±2%	
Wnat - 121	0,245	3	62	
Wnat – 120*	0,290	6	73	
Wnat – 109*	≥0,67	10	139	

* We were forced to reject the data of Wnat120 and Wnat109 targets because the experiments show a very large deviation of fission rates (up to 200%) of this targets. One of us (V.D.) supposes that this deviation is caused by advanced target surface imperfections.

V. RESULTS AND DISCUSSION

Here, we present results obtained of processing the data of the measurements for four nuclei. The results obtained for plutonium and americium are given as ratios of fission cross-sections of these nuclei to that of ^{235}U. In so doing, we did not use the thickness of fissionable layers listed in Table 1. In Fig.14 we present the ratios normalized to cross-section integrals in the energy range 8.0 – 15.0 MeV to the same of ENDF/B-VI file.

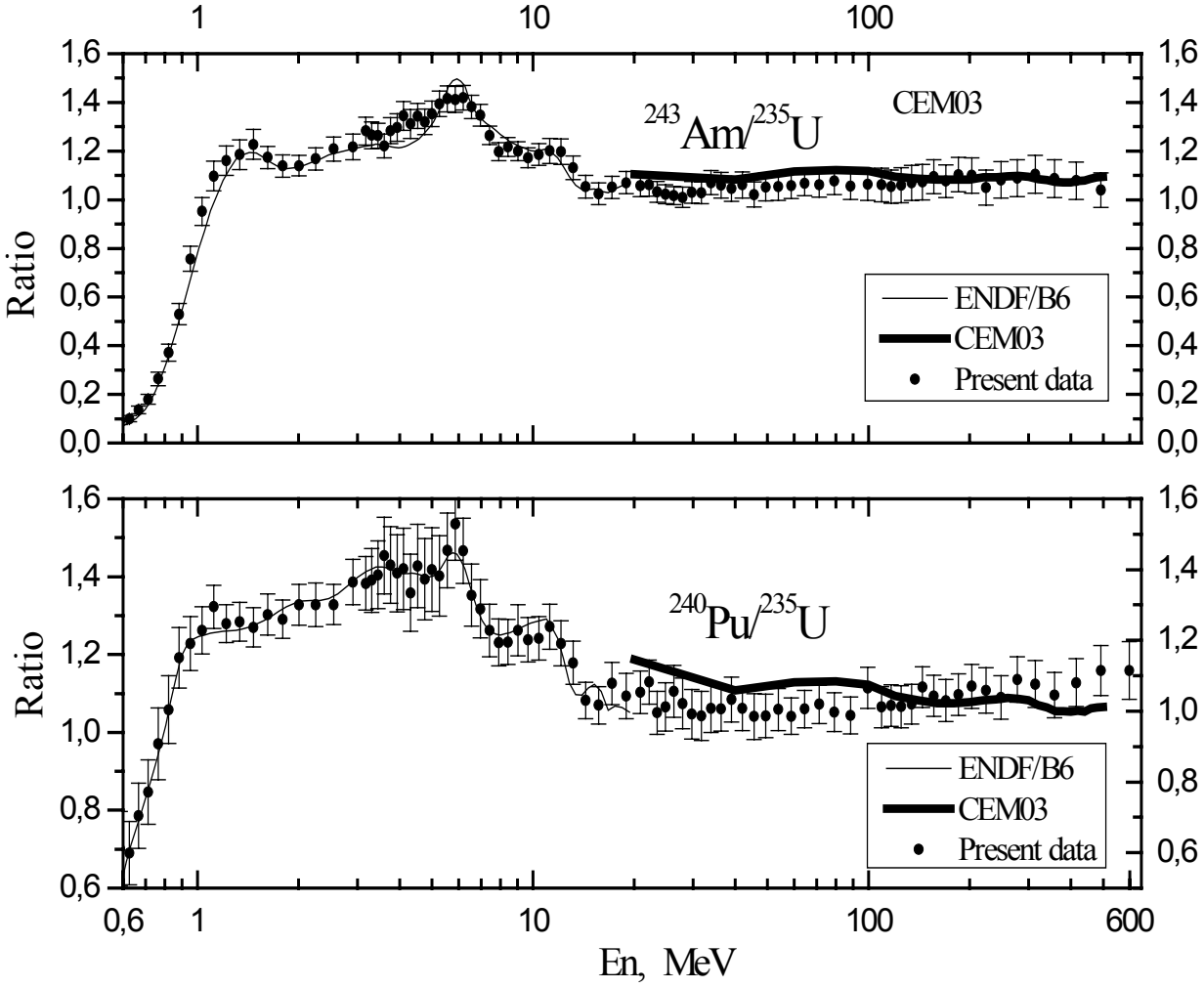

Fig. 14. Measured ratios normalized to the ENDF/B-VI reference data in the range 8.0–15.0 MeV compared with results by the CEM03 code [13].

Tabulated values of our data are presented in Tables 2 to 5. It is essential to note that the cross-section data in Tables 2-5 are averaged over energy channels; En [MeV] in the first column presents the middle value of the energy channel.

Table 2. Fission cross-section ratio of ^{240}Pu to ^{235}U, experimental data

En, MeV	Cross-section ratio	Uncertainty, %		
		Statistical	Systematical	Total
0.588	0.701	3.9	13.0	13.6
0.626	0.690	3.2	11.4	11.8
0.667	0.786	2.8	10.3	10.6
0.713	0.846	2.6	9.4	9.8
0.763	0.971	2.3	9.2	9.5
0.819	1.058	2.2	7.9	8.2
0.881	1.192	1.8	6.3	6.5
0.951	1.228	1.6	5.4	5.6
1.030	1.262	1.5	4.6	4.8
1.119	1.323	1.4	3.9	4.2
1.220	1.279	1.3	3.6	3.8
1.334	1.284	1.3	3.7	3.9
1.466	1.270	1.2	3.8	4.0
1.619	1.303	1.1	3.9	4.1
1.796	1.291	1.1	3.7	3.8
2.005	1.328	1.0	3.8	3.9
2.252	1.328	1.0	4.1	4.2
2.548	1.328	1.0	3.8	3.9
2.906	1.386	1.0	4.1	4.2
3.173	1.383	1.9	4.6	5.0
3.306	1.391	2.0	5.5	5.9
3.447	1.405	1.9	5.9	6.2
3.598	1.454	1.9	6.5	6.8
3.759	1.430	2.0	6.6	6.9
3.930	1.409	2.0	6.7	7.0
4.114	1.420	2.0	7.1	7.3
4.312	1.359	2.0	7.0	7.3
4.524	1.428	2.0	7.2	7.5
4.751	1.393	2.0	7.2	7.5
4.997	1.418	2.0	7.3	7.6
5.262	1.402	2.0	7.1	7.4
5.549	1.467	2.0	6.2	6.5
5.860	1.535	1.9	5.7	6.1
6.198	1.466	1.8	5.4	5.7
6.566	1.353	1.8	5.6	5.9
6.968	1.317	1.7	5.4	5.7
7.409	1.262	1.7	5.1	5.4
7.893	1.231	1.7	4.6	4.9
8.426	1.232	1.7	4.4	4.7
9.015	1.262	1.7	4.9	5.2
9.669	1.238	1.7	4.3	4.6
10.40	1.242	1.8	4.2	4.5
11.21	1.272	1.8	4.2	4.6

12.12	1.229	1.8	4.4	4.7
13.16	1.179	1.8	4.3	4.7
14.33	1.082	1.9	3.9	4.3
15.66	1.070	1.8	4.1	4.5
17.19	1.126	1.8	4.5	4.8
18.96	1.093	1.8	5.0	5.4
20.89	1.103	2.2	4.5	5.0
22.17	1.130	2.4	4.4	5.0
23.43	1.050	2.4	4.7	5.3
24.80	1.065	2.3	5.4	5.8
26.30	1.105	2.2	5.6	6.1
27.94	1.074	2.2	5.6	6.0
29.74	1.047	2.2	5.6	6.1
31.72	1.042	2.2	5.7	6.1
33.91	1.061	2.1	5.5	5.8
36.35	1.061	2.0	5.0	5.4
39.05	1.084	2.0	4.9	5.3
42.07	1.062	1.9	5.0	5.3
45.49	1.041	1.9	5.3	5.7
49.34	1.042	1.9	5.0	5.4
53.72	1.059	1.8	4.8	5.1
58.72	1.042	1.8	4.1	4.4
64.49	1.060	1.7	4.2	4.6
71.18	1.072	1.6	4.3	4.6
79.02	1.052	1.6	4.4	4.7
88.29	1.044	1.6	4.3	4.5
99.39	1.114	1.5	4.5	4.7
109.15	1.065	2.1	4.5	5.0
116.58	1.069	2.1	4.6	5.0
124.86	1.066	2.1	4.7	5.1
134.11	1.073	2.1	4.3	4.8
144.51	1.116	2.0	4.2	4.7
156.28	1.094	2.0	4.4	4.9
169.67	1.082	2.0	4.6	5.0
185.04	1.096	2.0	4.4	4.9
202.82	1.119	2.0	4.6	5.1
223.60	1.108	2.0	4.8	5.2
248.19	1.090	2.1	4.7	5.1
277.67	1.136	2.1	4.7	5.2
313.64	1.124	2.2	4.9	5.4
358.45	1.096	2.4	4.8	5.4

Table 3. Fission cross-section ratio of ^{243}Am to ^{235}U, experimental data

En, MeV	Cross-section ratio	Uncertainty, %		
		Statistical	Systematical	Total
0.588	0.090	9.1	11.4	14.6
0.626	0.100	7.0	10.6	12.7
0.667	0.136	5.6	10.7	12.0
0.713	0.179	4.7	10.4	11.4
0.763	0.264	3.7	9.9	10.6
0.820	0.372	3.1	8.8	9.3
0.882	0.530	2.3	8.0	8.4
0.952	0.757	1.7	6.5	6.7
1.030	0.952	1.5	5.8	6.0
1.119	1.097	1.3	5.5	5.6
1.220	1.160	1.2	5.0	5.2
1.334	1.185	1.1	5.1	5.2
1.466	1.227	1.1	4.9	5.0
1.619	1.174	1.0	3.8	3.9
1.796	1.139	1.0	3.9	4.0
2.005	1.140	1.0	3.5	3.6
2.252	1.168	0.9	3.8	4.0
2.548	1.208	0.9	4.0	4.1
2.906	1.217	0.9	4.2	4.3
3.173	1.283	1.7	4.2	4.5
3.306	1.265	1.8	4.0	4.3
3.447	1.263	1.7	3.8	4.1
3.598	1.221	1.8	3.6	4.0
3.759	1.284	1.8	3.7	4.1
3.930	1.297	1.8	3.9	4.3
4.114	1.345	1.7	4.1	4.4
4.312	1.312	1.8	4.2	4.5
4.524	1.344	1.7	3.5	3.9
4.751	1.320	1.7	3.6	4.0
4.997	1.354	1.7	3.5	3.9
5.262	1.394	1.7	3.3	3.8
5.549	1.414	1.7	3.4	3.8
5.860	1.412	1.7	3.3	3.7
6.198	1.420	1.6	3.2	3.5
6.566	1.382	1.5	3.1	3.4
6.968	1.347	1.4	2.9	3.3
7.409	1.265	1.4	2.7	3.0
7.893	1.198	1.5	2.7	3.1
8.426	1.217	1.4	2.8	3.2
9.015	1.200	1.5	2.9	3.3
9.669	1.172	1.5	3.1	3.5
10.397	1.186	1.5	3.5	3.8
11.211	1.201	1.6	4.0	4.3

12.125	1.198	1.6	4.0	4.3
13.156	1.132	1.6	4.0	4.3
14.326	1.054	1.6	4.1	4.4
15.660	1.024	1.6	4.1	4.4
17.192	1.051	1.6	4.1	4.4
18.963	1.070	1.6	4.0	4.3
20.888	1.058	1.9	3.9	4.3
22.169	1.062	2.1	3.9	4.4
23.429	1.032	2.1	3.5	4.1
24.800	1.023	2.0	3.3	3.8
26.298	1.017	2.0	3.0	3.6
27.937	1.010	2.0	3.7	4.2
29.738	1.031	1.9	3.9	4.3
31.721	1.028	1.9	3.9	4.3
33.913	1.070	1.8	4.3	4.7
36.345	1.060	1.8	4.6	5.0
39.055	1.045	1.7	4.6	4.9
42.086	1.061	1.7	4.7	5.0
45.494	1.021	1.7	4.8	5.1
49.345	1.052	1.6	5.1	5.4
53.721	1.053	1.6	5.1	5.3
58.725	1.057	1.5	4.7	5.0
64.489	1.068	1.5	4.4	4.7
71.181	1.062	1.4	4.6	4.8
79.018	1.076	1.4	5.0	5.2
88.290	1.056	1.3	5.1	5.3
99.391	1.063	1.3	6.0	6.2
109.146	1.061	1.8	6.2	6.5
116.583	1.054	1.8	6.2	6.5
124.858	1.060	1.8	6.5	6.7
134.112	1.069	1.8	6.5	6.7
144.514	1.072	1.8	6.5	6.7
156.278	1.094	1.7	6.1	6.4
169.671	1.076	1.8	6.0	6.2
185.037	1.103	1.7	6.2	6.4
202.818	1.100	1.8	6.4	6.6
223.604	1.050	1.8	6.6	6.8
248.188	1.081	1.8	6.6	6.9
277.674	1.090	1.9	6.7	7.0
313.642	1.104	1.9	6.8	7.1
358.447	1.087	2.1	6.9	7.2

In Tables 2 and 3, the total error of measurements is divided into statistical and systematic components. The systematic error was estimated from the

discrepancy in the curve shapes for the ratio of cross-sections obtained in several series of measurements and data treatments under varied requirements. In order to take account of correlation between data from different series, we apply the median filtering. As a rule, an estimation of systematic errors gave bigger values than the values obtained from the sum of errors of corrections. It is essential to note that the systematic error is not a true second moment of a distribution; our systematic error is evaluated from the distribution width only.

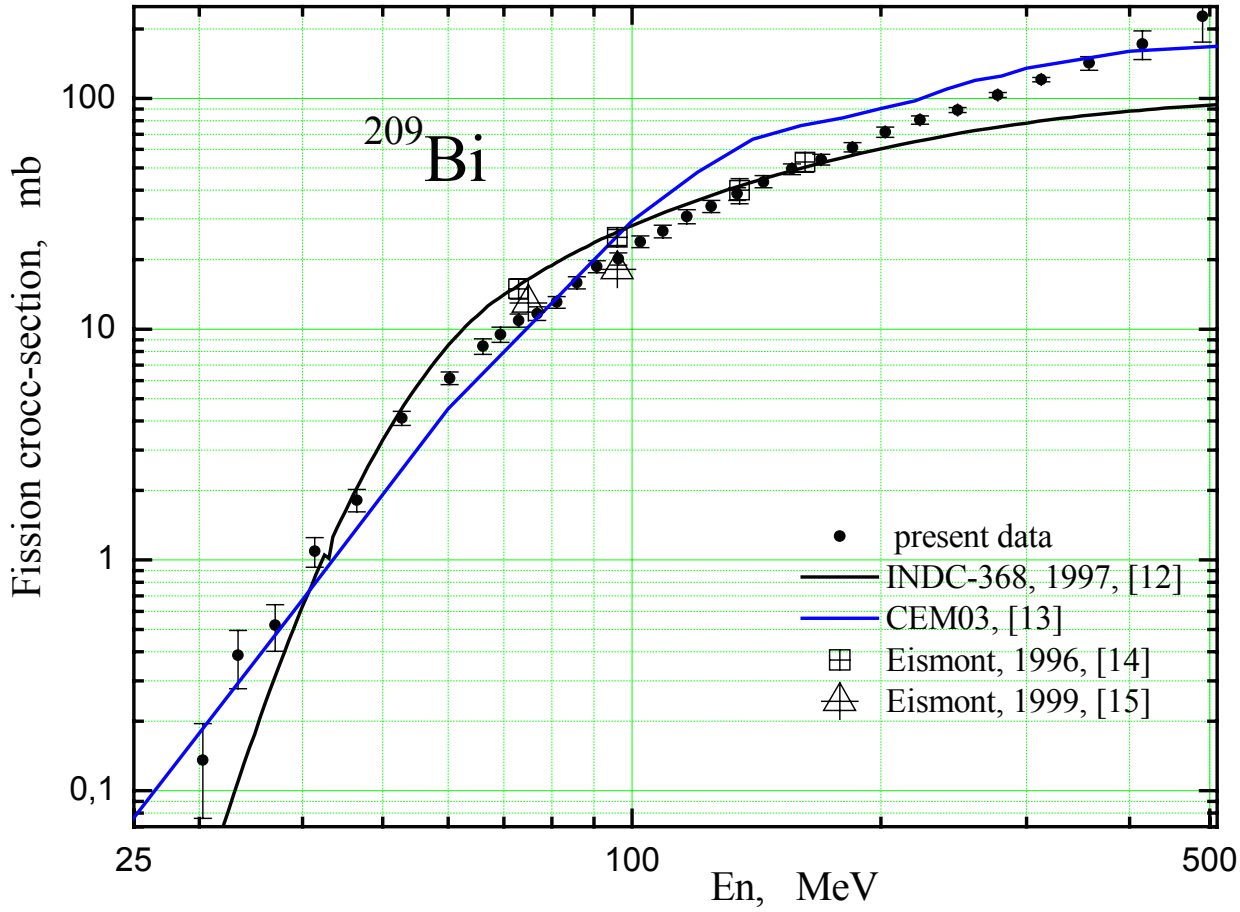

Fig. 15. Comparison of our measured bismuth fission cross-section with calculations by the code CEM03 (upper curve at the high energy end) and measurements by other authors.

For bismuth and tungsten the cross-sections are given in millibarns. To obtain these values, we have used a measured thickness of fissionable layers listed in Table 1. Therefore, our results are based on only recommended values of fission

cross-section of ^{235}U [12]. The approximation [12] given in Fig. 14 includes results of all previous literature data. For energy region above 100 MeV, due to energy dependences of cross-section (increasing) and neutron flux (decreasing), the weighted average value of the middle point of the energy interval is a little less than En by about 5-10%.

Table 4. Fission cross-section of ^{209}Bi, experimental data

En, MeV			σ_f, mb	Uncertainty, mb		
The Begin	The Middle	The End		Systematical	Statistical	Total
28.82	30.27	31.72	0.136	0.003	0.06	0.06
31.72	33.40	35.09	0.387	0.003	0.10	0.11
35.09	37.06	39.04	0.522	0.004	0.12	0.12
39.04	41.38	43.72	1.093	0.001	0.16	0.16
43.72	46.52	49.31	1.819	0.002	0.20	0.20
49.31	52.70	56.09	4.116	0.095	0.28	0.29
56.09	60.25	64.42	6.141	0.195	0.32	0.38
64.42	66.05	67.63	8.447	0.176	0.62	0.65
67.63	69.36	71.09	9.475	0.295	0.64	0.71
71.09	72.96	74.83	10.91	0.249	0.68	0.72
74.83	76.86	78.89	11.70	0.385	0.69	0.79
78.89	81.10	83.31	13.11	0.312	0.71	0.77
83.31	85.72	88.13	15.94	0.589	0.76	0.96
88.13	90.76	93.39	18.67	0.809	0.80	1.14
93.39	96.28	99.17	20.17	0.910	0.83	1.23
99.17	102.35	105.54	24.00	1.15	0.86	1.43
105.54	109.06	112.57	26.59	1.42	0.90	1.68
112.57	116.48	120.38	30.81	1.92	0.96	2.14
120.38	124.73	129.08	34.06	1.74	0.99	2.0
129.08	133.96	138.83	38.61	2.13	1.04	2.38
138.83	144.32	149.82	43.56	2.38	1.09	2.62
149.82	156.05	162.28	49.42	2.36	1.19	2.64
162.28	169.40	176.52	54.45	2.71	1.20	2.96
176.52	184.71	192.90	61.42	2.52	1.29	2.83
192.90	202.42	211.94	71.47	3.25	1.43	3.55
211.94	223.12	234.29	80.79	2.99	1.54	3.36
234.29	247.58	260.86	89.05	1.67	1.60	2.31
260.85	276.90	292.94	103.60	1.57	1.86	2.44
292.94	312.65	332.36	120.64	1.50	2.05	2.54
332.36	357.15	381.94	142.15	9.47	2.42	9.77
381.94	414.03	446.12	171.76	24.5	3.09	24.7

In Table 4, the total error is divided into two components, systematic and statistical. Here, as in the case of plutonium and americium, the systematic error was estimated from the discrepancy of the shape of measured dependences obtained in various series of measurements. The greatest correction in data processing was the correction for amplitude discrimination. It does not exceed 12% and cannot explain the difference between measuring series reaching 5%. One probable source of errors is lying in the instability of the cyclotron systems operating the proton beam, namely the system knocking off the accelerated beam of 1 GeV protons to throw it onto the neutron-producing target. As a result, a wrong start of the time-of flight system can arise.

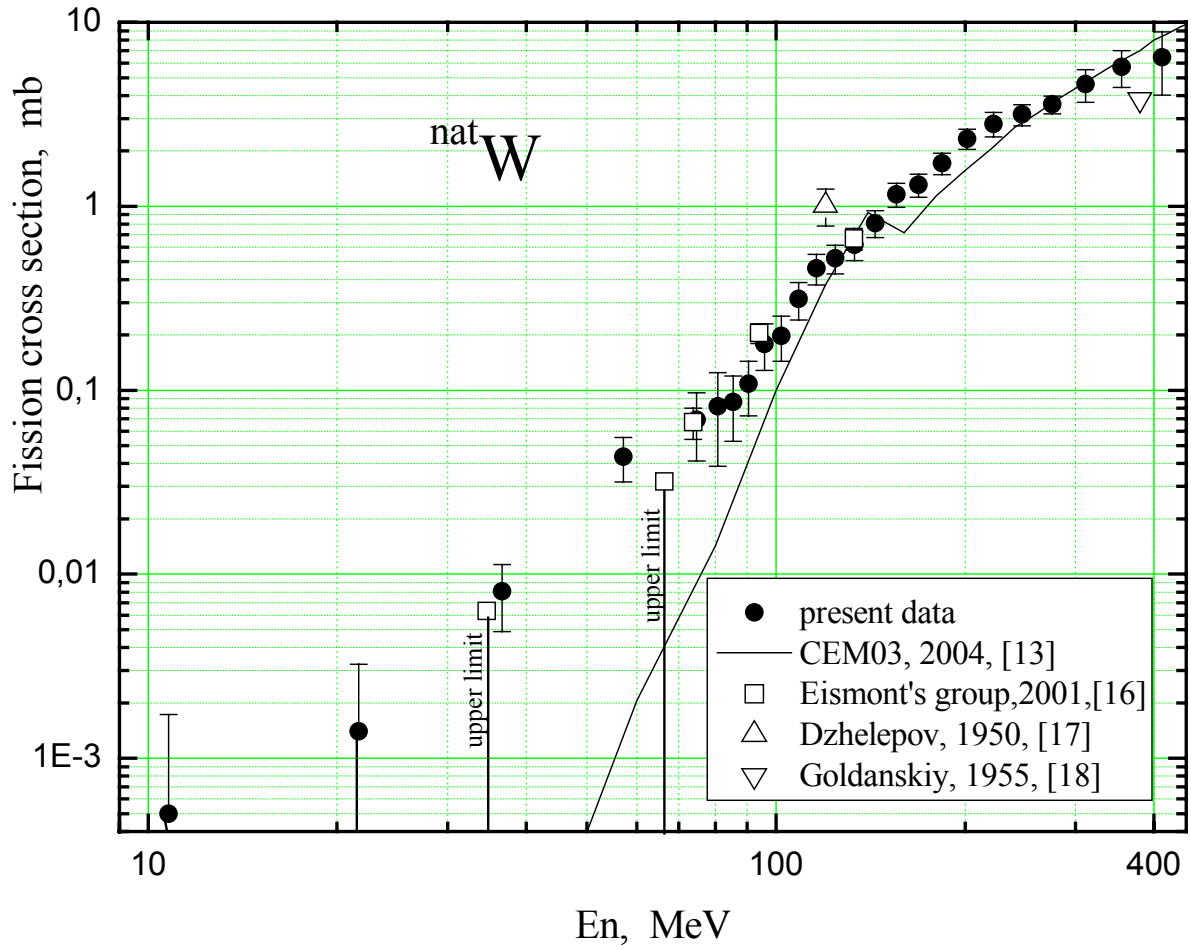

Fig. 16. Comparison of our results on measurement of tungsten fission cross-section with the improved Cascade-Exciton Model (code CEM03) calculations and measurements of other authors.

Table 5. Fission cross-section of ^{nat}W, experimental data

En, MeV		σ_f, mb	Uncertainty, %			
The Middle	Interval width		Target	Systematical	Statistical	Total
21.65	16.96	0.0014	7.0	0.5	131.0	131.2
36.60	13.93	0.0081	7.0	1.7	39.0	39.7
57.19	27.26	0.0436	7.0	3.2	26.3	27.4
74.71	7.78	0.0690	7.0	11.8	37.9	40.3
80.79	4.40	0.0818	7.0	17.2	49.3	52.7
85.39	4.80	0.0862	7.0	16.6	34.3	38.8
90.41	5.24	0.1082	7.0	7.4	31.3	32.9
95.91	5.76	0.1788	7.0	13.4	23.7	28.1
101.96	6.34	0.1982	7.0	8.4	24.9	27.2
108.63	7.00	0.3129	7.0	8.1	20.4	23.1
116.01	7.77	0.4618	7.0	5.6	16.7	19.0
124.23	8.66	0.5213	7.0	4.5	15.9	17.9
133.42	9.71	0.6180	7.0	5.2	15.4	17.7
143.74	10.94	0.8107	7.0	6.3	13.8	16.7
155.41	12.40	1.1611	7.0	5.5	11.9	14.9
168.70	14.16	1.3076	7.0	5.4	11.2	14.3
183.93	16.30	1.7115	7.0	5.7	9.7	13.3
201.55	18.94	2.3331	7.0	5.9	8.5	12.5
222.14	22.23	2.8105	7.0	10.8	8.3	15.3
246.47	26.43	3.1580	7.0	7.8	7.9	13.1
275.63	31.89	3.5785	7.0	3.7	7.6	11.0
311.16	39.18	4.5999	7.0	17.4	7.3	20.1
355.37	49.24	5.7246	7.0	20.4	7.0	22.7

As comments to Fig. 16, the following remarks should be made: (1) ^{nat}W present a mixture of five isotopes ^{186}W, ^{184}W, ^{183}W, ^{182}W, and ^{180}W, having approximately equal (except of ^{180}W), natural abundance. Since the fission cross-section is governed by the fission barrier (calculated values are from 16.2 to 17.7 MeV for 100 MeV neutrons, i.e., nuclear excitation energy about 60 MeV), it is difficult to expect that the cross-section of each of the component differs considerably from their natural mixture (moreover, taking into account preceding multiple nucleon evaporation: about 4 and 6 nucleons for 100 and 200

MeV neutrons, accordingly). (2) The extremely low (fractions of millibarn) value of the cross-section of tungsten opens up opportunities to obtain data on the competitive with the fission reactions. Opening or closing of channels of these reactions should be reflected on the run of dependence of tungsten fission

VIII. CONCLUSIONS

Our accuracy of the shape measurements is about 3 – 5 %. It is limited at this level by the stability level of the cyclotron systems governing the accelerated proton's beam.

In order to expand the energy range towards higher energy and to get reliable data for E_n >200 MeV, one needs to modernize the electronics of the measuring unit: a) To increase the operation frequency of time-to-digit converters from 100 MHz up to 300 – 600 MHz; b) To do the common start of the time-to-digit converters by a single quartz generator.

One can measure fission cross-sections of the alpha-radioactive nuclei with lifetimes less than 10 000 years (like Pu-238, -241 or Am-241), if the fission detector is switched into the avalanche mode of operation. This detector also needs smaller corrections for the neutron flux distortion, which is essential for measurements in the energy range lower than 0.1 MeV.

A numerical model of the experimental amplitude spectra (of the fragments and background charged particles) allows measuring nuclides with extra-low fissility, such as tungsten, tantalum, gold, lead and bismuth.

The improved Cascade-Exciton Model (CEM) as realized in the code CEM03 allows us to describe well all the measured here fission cross sections, except for the low energy part (En < 100 MeV) of the tungsten data, underestimated by CEM03.

Acknowledgments

This work was partially supported by the US Department of Energy, the Moldovan-US Bilateral Grants Program, CRDF Project MP2-3045, and the NASA ATP01 Grant NRA-01-01-ATP-066.

REFERENCES

[1]. N. K. Abrosimov, G. Z. Borukhovich, A. V. Laptev, V. V. Marchenkov, G. A. Petrov, O. A. Shcherbakov, Yu. V. Tuboltsev, V. I. Yurchenko, Nucl. Instrum. Methods, **A242,** 121-133 (1985).

[2] ENDF/B-VI, Release 7., UCRL-ID-127776, Rev. 1б, A Temperature Dependent ENDF/B-VI, Release 7 Cross Section Library, D.E. Cullen University of California Lawrence Livermore National Laboratory, Livermore, Nov 22, 2000.

[3] Turchin V.F., Kozlov V.P., Malkevich M.S., The Use of Methods of Mathematical Statistics for Solving Ill-Conditioned Problems, Usp. Fiz. Nauk, **102,** No. 3, 345-386 (1970).

[4] D. H. Wright, GEANT4 Toolkit, "Physics Reference Manual", December 5, 2003, CERN, Program Library.

[5] Shiori Furihata, "Development of a Generalized Evaporation Model and Study of Residual Nuclei Production," PhD thesis, Tohoku University, March 2003, and references therein.

[6] S. Furihata, "The GEM Code – The Generalized Evaporation Model and the Fission Model," Proc. Int. Conf. on Advanced Monte Carlo for Radiation Physics, Particle Transport Simulation and Applications, 23-26 Oct. 2000, Lisbon, Portugal, Springer Verlag, Berlin-Heidelberg (2000) 1045-1050.

[7] G. Audi and A. H. Wapstra, "The 1995 Update to the Atomic Mass Evaluation," Nuclear Physics, **A595**, No. 4, 409-480 (1995); masses recommended.

[8] J. W. Truran, A. G. W. Cameron, E. Hilf, Proc. Int. Conf. on the Properties of Nuclei Far From the Beta-Stability, Leysin, Switzerland, August 31 - September 4, 1970, Vol. 1, p. 275.

[9] Yu. P. Gangrskii, B. N. Makarov, and V. P. Perelygin, *Registration and Spectrometry of Fission Fragments,* Moscow, Energoatomizdat, 1981 (in Russian); James F. Ziegler, "SRIM2003, The Stopping and Range of Ions in Matter, Group of Programs Instruction Manual" IBM-Research, 28-0, Yorktown, NY, 10598, USA.

[10] A. Fasso, A. Ferrari, J. Ranft, P. R. Sala, "FLUKA: Status and Prospective for Hadronic Applications", Proceedings of the Monte Carlo 2000 Conference, Lisbon, October 23-26 2000, A. Kling, F.Barao, M. Nakagawa, L. Tavora, P. Vazeds, Springer-Verlag Berlin, p.955-960 (2001).

[11] S. M. Soloviev, Calibration of Heavy-Element Nuclear Targets by Rutherford Backscattering of Alpha Particles, Nuclear Instruments and Methods in Physics Research, **A397**, 159-162 (1997).

[12] A. D. Carlson, S. Chiba, F.-J. Hambsch, N. Olsson, A. N. Smirnov, "Update to Nuclear Data Standards for Nuclear Measurements," INDC(NDS)-368, Vienna, May 1997.

[13] S. G. Mashnik, K. K. Gudima, I. V. Moskalenko, R. E. Prael, A. J. Sierk, "CEM2K and LAQGSM Codes as Event Generators for Space-Radiation-Shielding and Cosmic-Ray-Propagation Applications," Advances in Space Research, **34,** 1288–1296 (2004); S. G. Mashnik, K. K. Gudima, A. J. Sierk, R. E. Prael, "Improved Intranuclear Cascade Models for the Codes CEM2k and LAQGSM," LANL Report LA-UR-05-0711, E-print: nucl-th/0502019, Proc. Int. Conf. on Nuclear Data for Science and Technology (ND2004), September 26 – October 1, 2004, Santa Fe, USA.

[14] V. P. Eismont, A. V. Kireev, I. V. Ryzhov, S. M. Soloviev, G. A. Tutin, H. Conde, K. Elmgren, N. Olsson, and P.-U. Renberg, "Neutron-Induced Fission Cross Section Ratios of ^{209}Bi to ^{238}U at 75 and 96 MeV," Proc. 3rd Int. Conf. on Accelerator-Driven Transmutation Technologies and Applications, Praha, Czech Republic, June 7-11, 1999 (CD ROM publication, paper Mo-O-C7).

[15] V. P. Eismont, A. V. Prokofiev, A. N. Smirnov, K. E. Elmgren, J. Blomgren, H. Conde, J. Nelson, N. Olsson, T. Ronnqvist, E. Traneus, Phys. Rev., **C53**, 2911 (1996).

[16] Taken from the dissertation by A. Prokofiev, Uppsala Univ. 2001, p. 23; A. V. Prokofiev, P.U. Renberg, and N. Olson, "Measurement of Neutron-Induced Fission Cross Sections for ^{nat}Pb, ^{208}Pb, ^{197}Au, ^{nat}W, and ^{181}Ta in the Intermediate Energy Region," UU-NF 01#6, Uppsala University Neutron Physics Report ISSN 1401-6269 (March 2001).

[17] V. P. Dzhelepov, B. M. Golovin, Ju. M. Kazarinov, Report of Inst. of Nuclear Problems Academy of Science, USSR, 1950, taken from Ref. [18].

[18] V. I. Goldanskiy, E. Z. Tarumov, V. S. Penkina, "Fission of Heavy Nuclei by Neutrons of High Energy", Dokl. Akad. Nauk, **101,** 1027-1030 (1955).